Journal of Power Sources 246 (2014) 912–917

Contents lists available at ScienceDirect

Journal of Power Sources

journal homepage: www.elsevier.com/locate/jpowsour

Preparation and electrochemical properties of high-capacity $LiFePO_4$–$Li_3V_2(PO_4)_3$/C composite for lithium-ion batteries

Yong Guo [a], Yudai Huang [a], Dianzeng Jia [a,*], Xingchao Wang [a], Neeraj Sharma [b], Zaiping Guo [c], Xincun Tang [a]

[a] Key Laboratory of Material and Technology for Clean Energy, Ministry of Education, Key Laboratory of Advanced Functional Materials, Autonomous Region, Institute of Applied Chemistry, Xinjiang University, Urumqi 830046, Xinjiang, China
[b] School of Chemistry, The University of New South Wales, Sydney, NSW 2052, Australia
[c] Institute for Superconducting & Electronic Materials, University of Wollongong, NSW 2522, Australia

HIGHLIGHTS

- A matrix is formed by conductive carbon surrounding the LFP–LVP particles.
- LFP–LVP/C is composed of V-doping into LFP, LVP and mixed phase of V-doped LFP and LVP.
- Formation of LFP–LVP/C improves the electronic conductivity and Li^+ diffusion.

ARTICLE INFO

Article history:
Received 7 May 2013
Received in revised form
19 July 2013
Accepted 14 August 2013
Available online 27 August 2013

Keywords:
High-capacity
Lithium iron phosphate–lithium vanadium phosphate/carbon composite
Cathode material
Lithium-ion batteries

ABSTRACT

$LiFePO_4$–$Li_3V_2(PO_4)_3$/C (LFP–LVP/C) composite is prepared by a modified solid-state method, along with LFP/C composite as a reference. The structure and morphology of the as-prepared materials are analyzed by X-ray diffraction (XRD) and electron microscopy. LFP–LVP/C composite is well-crystallized and a matrix is formed by conductive carbon surrounding the LFP–LVP particles. LFP–LVP/C exhibits V-doped LFP in the bulk phase as determined by Rietveld analysis of XRD data, and mixed phase regions of V-doped LFP and LVP when analyzed at the particle-scale using high-resolution transmission electron microscopy. Electrochemical tests show that the initial discharge capacity of the LFP–LVP/C composite is 165.2 mAh g^{-1} at 0.1 C. Furthermore, the composite exhibits excellent performance with an initial discharge capacity of 135.4 mAh g^{-1} at a constant current density of 1 C, with no noticeable capacity fading after 100 cycles (141.6 mAh g^{-1}), which is higher than that of LFP/C prepared by the same method for comparison. Thus, the introduction of LVP acts to improve electronic conductivity and Li^+ diffusion of LFP/C.

© 2013 Elsevier B.V. All rights reserved.

1. Introduction

Polyanion phosphate cathode materials have attracted great interest since the first report on the electrochemical performance of olivine-type $LiFePO_4$ (LFP) Padhi et al. [1]. These cathodes feature strong P–O bonds and a three-dimensional solid framework of PO_4^{3-} anions, which result in higher thermal stability than conventional layered transition-metal oxides used as cathodes in lithium-ion batteries. This in turn makes polyanion phosphate cathodes more suitable for large-scale lithium-ion battery applications, such as in electric vehicles (EVs) and hybrid electric vehicles (HEVs) [2,3]. LFP is recognized as a promising polyanion phosphate cathode material for lithium-ion batteries due to its high theoretical capacity (170 mAh g^{-1}), cycling stability, low cost and environmental friendliness. However, LFP usually shows a poor rate capability because of its low intrinsic electronic conductivity (10^{-7}–10^{-9} S cm^{-1}) and slow Li^+ diffusion (10^{-16} cm^2 s^{-1}) [4,5]. Monoclinic lithium vanadium phosphate (LVP) is an alternative promising phosphate cathode material for lithium-ion batteries application due to its good ion mobility, high operating voltage, high capacity and the reversibility of capacity in subsequent cycles [6]. LVP has attracted considerable attention for its improved lithium-ion conduction properties relative to other members in the phosphate cathode family owing to the fact that Li^+ can transfer faster in its more open three-dimensional framework than the Li^+ transfer

* Corresponding author. Tel./fax: +86 991 8588209.
E-mail addresses: jdz@xju.edu.cn, jdz0991@gmail.com (D. Jia).

0378-7753/$ – see front matter © 2013 Elsevier B.V. All rights reserved.
http://dx.doi.org/10.1016/j.jpowsour.2013.08.047

observed in the more restricted olivine-structure [7]. However, the intrinsic low electronic conductivity (2.4×10^{-7} S cm^{-1}) of LVP critically limits its high rate performance [8]. In this report, we combine the above mentioned polyanionic phosphate cathodes and synthesize LFP–LVP particles coated with conductive carbon, to address whether this is an effective method of improving the electrochemical performance above that of a single-phase LFP or LVP cathode.

Ma et al. [9] studied the effect of vanadium on the physiochemical and electrochemical performance for LFP synthesized by the sol–gel method. They observe the formation of different impurity phases (VO_2 or LVP phases), which further increases the electrical conductivity of LFP. Yang et al. [10] reported the synthesis of carbon coated $LiFePO_4/Li_3V_2(PO_4)_3$ materials by the solution method, which exhibited a high discharge capacity. It has been reported that the synthesis of LFP–LVP particles coated with conductive carbon would be an effective method for achieving improved electrochemical performance [11]. However, to the best of our knowledge, no work has explored the LFP–LVP/C system in detail and investigated whether there is a formation of solid solutions or whether there is a reaction in the solid-state that incorporates V into LFP.

Our approach was to use a modified solid-state method, which features advantages of low energy consumption, convenient operation, and environmental friendliness. Moreover, it is a simple and effective method that can be scaled-up for commercial-scale materials fabrication. For instance, it has been employed in fabricating spinel $LiMn_2O_{3.9}Br_{0.1}$ nanoparticles [12], $LiMn_2O_{3.95}Br_{0.05}/SiO_2$ nanoparticles [13], and specifically, LFP-based cathode materials for electrode applications in lithium-ion batteries [14,15]. We extend this method to LFP–LVP/C and determine the synergistic effects of the LFP–LVP particles with nanostructured carbon, the structural characteristics and electrochemical performance of LFP–LVP/C composites.

2. Experimental

LFP–LVP/C composite was synthesized by solid-state reactions in combination with anhydrous ethanol. Lithium acetate dihydrate, iron (II) oxalate dihydrate, ammonium dihydrogen phosphate and ammonium metavanadate (Tianjin Yong Sheng Chemicals Co., LTD., China) with molar ratios of 1.02:0.95:1:0.05 were used as precursors. 2% excess Li was used to supplement the volatilization of Li at high temperature. An appropriate amount of dextrose dihydrate (8 wt% relative to total precursors) was added as carbon source and reducing agent. The starting materials and anhydrous ethanol were thoroughly mixed and milled in an agate mortar and pestle for 2 h, the materials experienced a modified solid-state reaction [14] to form a homogeneous fawn mixture. The mixture was initially heated in a tube furnace at 450 °C for 6 h, subsequently heating to 700 °C for 10 h under nitrogen and then cooled to room temperature. For comparison, LFP/C sample was prepared using the same procedure without ammonium metavanadate.

The crystal structures of the samples were investigated using a Bruker D8 Advance X-ray diffractometer with Cu Kα radiation. Rietveld analysis was performed using GSAS with the EXPGUI

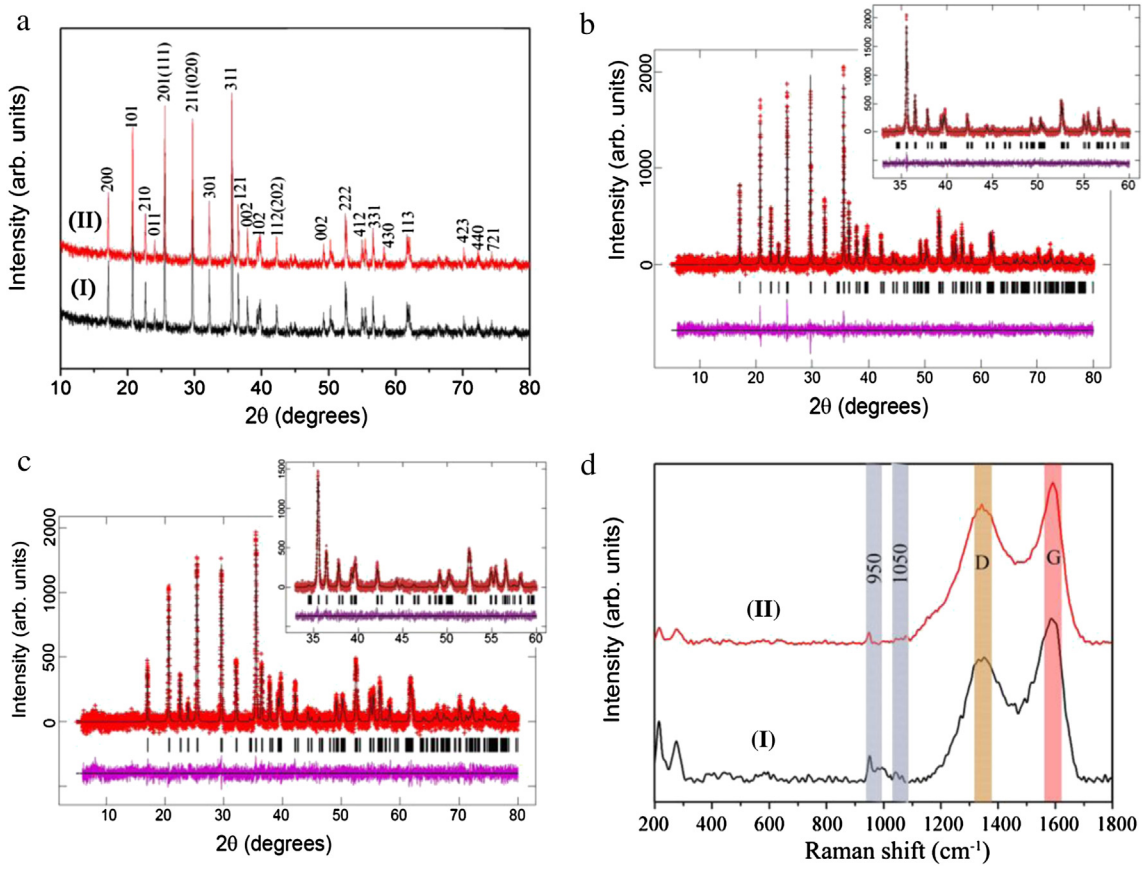

Fig. 1. (a) XRD patterns of LFP/C (I) and LFP–LVP/C (II) and Rietveld-refined fits of the $LiFePO_4$ and $Li_{1-x}V_xFePO_4$ structural models to XRD data of (b) LFP/C and (c) LFP–LVP/C. The red crosses are the data, black line through the crosses is the calculated model, the purple line at the bottom the difference between the data and calculated model and the black vertical lines are the Bragg reflection markers for the modeled phase. (d) Raman spectra of LFP/C (I) and LFP–LVP/C (II). (For interpretation of the references to colour in this figure legend, the reader is referred to the web version of this article.)

Table 1
Refined crystallographic parameters for $Li_{0.943(9)}V_{0.057(9)}FePO_4$, in *Pnma* space group symmetry using laboratory XRD data, with $a = 10.34564(25)$, $b = 6.01940(12)$ and $c = 4.70369(12)$ Å, with $R_p = 2.17\%$, $wR_p = 2.75\%$, and $\chi^2 = 0.87$ for 36 variables.

Atom	*x*	*y*	*z*	ADP (U_{iso})	Fractional occupancy
Li	0	0	0	0.092(18)[a]	0.943(9)[b]
V	0	0	0	0.092(18)[a]	0.057(9)[b]
Fe	0.2818(2)	0.25	0.9732(6)	0.0120(11)	1
P	0.0944(4)	0.25	0.4124(11)	0.0105(16)	1
O(1)	0.0943(11)	0.25	0.7306(21)	0.046(4)	1
O(2)	0.4543(10)	0.25	0.2143(13)	0.0040(25)	1
O(3)	0.1653(8)	0.0359(10)	0.2857(9)	0.0111(21)	1

[a] Constrained to be equal.
[b] Constrained to equal one.

interface [16,17]. The morphology was investigated by transmission electron microscopy (TEM, H-600, Hitachi, Japan), field emission scanning electron microscopy (FE-SEM, S-4800, Hitachi, Japan) and high-resolution transmission electron microscopy (HRTEM, 2100, JEM, Japan). The Raman spectra were measured by a Bruker Senterra R200-L spectrometer (532 nm). The electrical conductivities of the composites were measured at room temperature by a four-point probe resistivity measurement (RTS-9, Guangdong, China).

For electrochemical characterization, the working electrode was prepared by first making a cathode slurry by thoroughly mixing 85 wt% active materials, 10 wt% acetylene black, and 5 wt% poly (vinylidene fluoride) in *N*-methylpyrrolidinone solvent. Then, the obtained slurry was spread onto aluminum foil substrates and dried in a vacuum oven at 110 °C for 12 h. The cells consisted of the LFP/C or LFP–LVP/C composite as the positive electrode, a Li disk as the counter electrode, and an electrolyte composed of 1 M $LiPF_6$ in a 1:1 (volume ratio) mixture of ethylene carbonate and dimethyl carbonate. Celgard 2300 membrane was used as the separator. All cells were assembled in an argon-filled glove box, where water and oxygen concentration were kept less than 5 ppm. All electrochemical tests were carried out at room temperature. Cyclic voltammetry (CV, CHI660D, Chenhua, China) experiments were conducted at various scanning rates from 0.1 to 1 mV s^{-1} between 2.5 and 4.2 V. Charge/discharge tests were performed at constant current densities of 0.1–1 C within the potential range of 2.5–4.2 V. Electrochemical impedance spectroscopy (EIS) was measured on a Zahner Elektrik electrochemical workstation in the frequency range of 0.01–100 kHz, which applied a DC potential equal to the open circuit voltage of the cell and an AC oscillation of 5 mV.

3. Results and discussion

Fig. 1(a) shows the XRD patterns of the as-prepared LFP/C and LFP–LVP/C. Inspection of the patterns indicates that both samples produce well crystallized phases and no impurity phases are found. In both cases the major long-range ordered structure present was $LiFePO_4$ adopting orthorhombic *Pnma* space group symmetry [11]. The lattice for LFP/C was $a = 10.32684(20)$, $b = 6.00752(10)$ and $c = 4.69193(10)$ Å (Fig. 1(b)) while the lattice for LFP–LVP/C was expanded in all dimensions $a = 10.34564(25)$, $b = 6.01940(12)$ and $c = 4.70369(12)$ Å (Fig. 1(c)). This corresponds to 1.88(3), 1.18(2) and 1.18(2)% expansion in the *a*, *b*, and *c* lattice parameters of the LFP–LVP/C electrode relative to the LFP/C electrode. Such an expansion of the lattice is an indication that V-substitution is occurring into the LFP structure. Using only a LFP structural model, the refined crystallographic parameters of LFP/C show no evidence of anomalies, e.g. unrealistic bond lengths or atomic displacement parameters (ADP), while in LVP–LFP/C anomalies are observed. Interestingly, placing some vanadium on the lithium site in LVP–

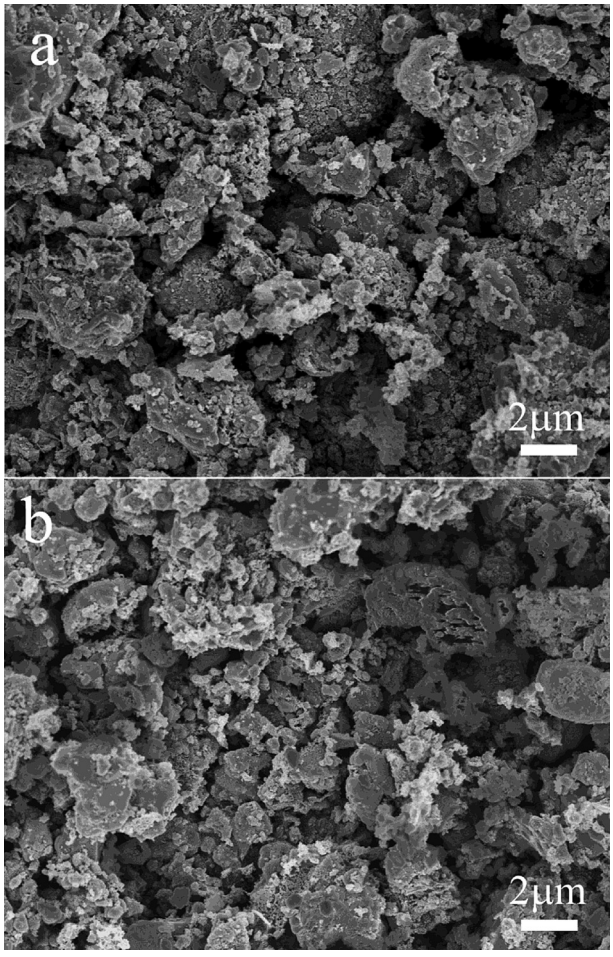

Fig. 2. SEM images of LFP/C (a) and LFP–LVP/C (b).

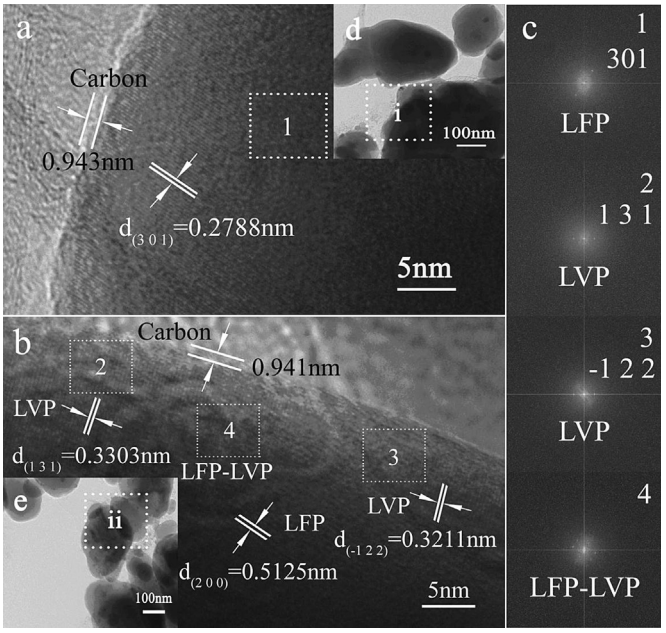

Fig. 3. HRTEM images of LFP/C (a) and LFP–LVP/C (b), with the selected areas i (d) and ii (e) of containing corresponding of TEM images. Fast Fourier transforms (FFT) (c) of the HRTEM images in the selected regions 1, 2, 3, and 4 of (a) and (b).

LFP/C and constraining their ADPs and the total site occupancy led to a reasonable model without anomalies and in addition a slight improvement in the fitting statistics. Furthermore, the vanadium content was allowed to refine leading to a composition of $Li_{0.943(9)}V_{0.057(9)}FePO_4$ and the crystallographic details are presented in Table 1. Vanadium substitution into LFP has been previously reported [18], however, the synthesis method used here differs from those reports. Including the LVP phase in the LFP–LVP/C refinements did not significantly improve the fit and the maximum fraction of LVP was 1.3(2)%. There is no evidence crystalline carbon present in either sample, presumably related to its amorphous nature or the predicted carbons layers on the active material particles being too small to be detected by the XRD [19]. Therefore, Rietveld analysis of XRD data illustrates that the LFP component of LFP–LVP/C has been modified to V-doped LFP and this would contribute the changes in performance. Analysis of XRD data also suggests that the LVP component is: in minute quantities, amorphous, nano-crystalline or forms a thin surface layer, all of which can be present and not necessarily detected by XRD data.

The Raman spectra of LFP/C and LFP–LVP/C (Fig. 1(d)) show a few bands due to the stretching of PO_4^{3-} groups, the bands appear around 950 and 1050 cm^{-1}, which are attributed to the vibrations of $v_1(PO_4^{3-})$ and $v_3(PO_4^{3-})$, respectively [20]. They also show the characteristic carbon signatures at ~1360 and ~1600 cm^{-1}, which match with the graphite band (G-band) and the disorder-induced phonon mode (D-band), respectively [21]. Additionally, the peak intensity ratio between D and G bands (I_D/I_G) generally provides an indication of the degree of crystallinity of various carbon materials, i.e., the smaller the ratio of I_D/I_G, the higher the degree of ordering in the carbon material [22]. In the present case, the I_D/I_G ratio is 0.85 and 0.84 for LFP/C and LFP–LVP/C, respectively, indicating that the coating mostly contains ordered carbon [23], which will be beneficial for achieving better electronic conduction between adjacent particles to enhance electrochemical performance.

SEM images of LFP/C and LFP–LVP/C are shown in Fig. 2(a) and (b). It can be seen that both samples contain some large particles due to the aggregation of the crystals in both cases.

The HRTEM image (Fig. 3(a)) shows that the LFP particles are wrapped with a thin layer of carbon (about 0.943 nm thick), which would offer a good electronic conductive network for the active materials. LFP exhibits regular lattice fringes of the (301) crystalline plane with measured *d* (inter-planar) spacing of 0.2788 nm. A similar sized carbon layer (about 0.941 nm thick) was found to be coated on the surface of LFP–LVP (Fig. 3(b)), which provides a similar effect on the electronic conductive network to that of LFP. There is evidence for two different lattices, one that can be associated with the lattice fringe of LFP (*d*-spacing of 0.5125 nm, lattice plane (200)), while the others measured to be 0.3303 and 0.3211 nm separately, which are compatible with the fringe spacing values of the (131) and (−122) planes of LVP (PDF#80-1515). The FFT images (Fig. 3(c)) of region 1 from Fig. 3(a) show diffraction spots corresponding to LFP. The FFT images of regions 2 and 3 from Fig. 3(b) correspond to the diffraction spots of LVP, while the FFT image of region 4 from Fig. 3(b) features diffraction spots from both

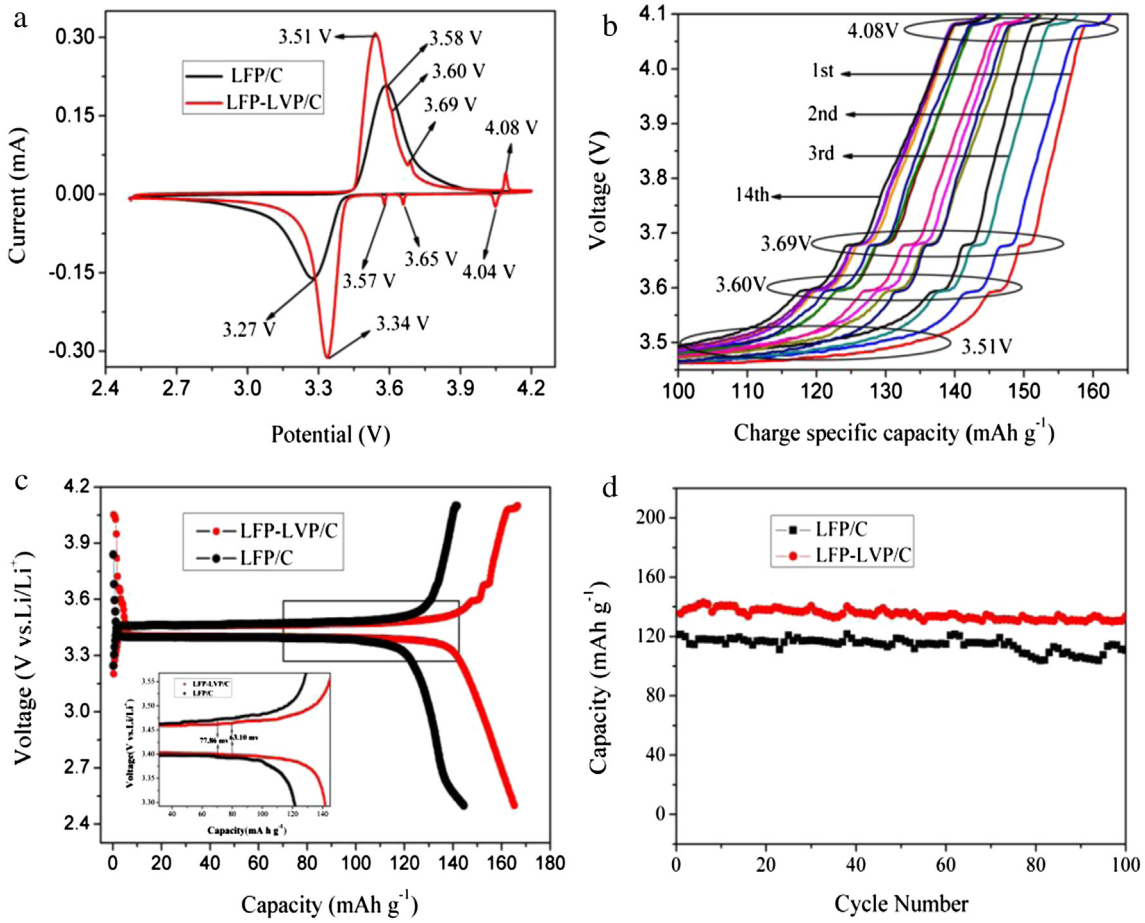

Fig. 4. (a) Cyclic voltammogram of LFP–LVP/C at a sweep rate of 0.1 mV s^{-1}. (b) The first fourteen charge profiles for LFP–LVP/C, data were collected at the rate of 0.1 C in the potential range of 2.5–4.2 V. (c) The initial charge/discharge curves of LFP–LVP/C and LFP/C at a current rate of 0.1 C, the inset shows the magnifications of selected regions. (d) Discharge capacity of LFP–LVP/C and LFP/C electrodes at 1 C in the voltage of 2.5–4.2 V.

LFP and LVP. These results demonstrate that the as-prepared materials form a composite composed of LFP–LVP/C. The three phases are clearly observed and initial indications based on HRTEM suggest a core of V-doped LFP, LVP, and V-doped LFP–LVP for the active material particles which are in turn dispersed in a shell of the matrix of carbon. The arrangement of this composite is likely to exhibit different channels of Li^+ diffusion and reaction mechanism evolution [24], especially in the mixed phase regions, due to the three-dimensional framework of NASICON-type LVP providing efficient three-dimensional Li^+ transport pathways and facile strain relaxation during battery charge and discharge. Moreover, conductive carbon wrapping on the LFP–LVP particles would further enhance the conductivity of the electrode, a synergistic effect which improves the electrochemical performance, as has been observed in previous papers [25,26].

Overall, bulk structural analysis based on Rietveld analysis of XRD data clearly illustrates a phase-pure LFP electrode for LFP/C, and a V-doped LFP electrode for LFP–LVP/C. Raman spectra and HRTEM data clearly illustrate a carbon matrix between the particles in each case. HRTEM data shows that the carbon layer thickness is equivalent in both electrodes and that the LFP/C cathode is comprised of LFP while the LFP–LVP/C cathode is comprised of regions of LFP (V-doped LFP from XRD data analysis), LVP, and mixed regions of V-doped LFP and LVP. Therefore, the differences in LFP/C and LFP–LVP/C are: V-doping into LFP, LVP, and the mixed phase regions of V-doped LFP and LVP. Thus, any difference in the electrochemical performance of LFP/C and LFP–LVP/C electrodes can be related to these two differences.

The electronic conductivities of the LFP/C and LFP–LVP/C are measured at room temperature using a four-point probe resistivity measurement which results in values of 8.94×10^{-4} S cm^{-1} and 2.65×10^{-3} S cm^{-1}, respectively.

The cyclic voltammogram curves of LFP–LVP/C and LFP/C between 2.5 and 4.2 V at a scan rate of 0.1 mV s^{-1} are presented in Fig. 4(a). The redox peaks at about 3.58/3.27 V for LFP/C and 3.51/3.34 V for LFP–LVP/C correspond to the two-phase charge–discharge reaction of the Fe^{2+}/Fe^{3+} redox couple [27]. The LFP–LVP/C cathode possesses a higher pair of current peaks corresponding to reactions of LFP, and the potential difference between the anodic and cathodic peaks for the LFP–LVP/C relative to the LFP/C electrode decreases dramatically from 0.31 to 0.17 V. This decrease in potential difference can be ascribed to the faster ion conduction observed in LVP [2]. LFP–LVP/C possesses better reversibility and better kinetic behavior compared to LFP/C electrodes. The four anodic peaks of LFP–LVP/C match well with the four charge plateaus shown in Fig. 4(b). One pair of redox peaks in the CV curves, located at 3.51/3.34 V, corresponds to reaction of $Fe^{2+} \leftrightarrow Fe^{3+}$ ($LiFePO_4 \leftrightarrow FePO_4$), the other three pairs of redox peaks in the CV curves, located at 3.60/3.57 V, 3.69/3.65 V and 4.08/4.04 V, correspond to the more complex phase changes in LVP associated with $V^{3+} \leftrightarrow V^{4+}$ presumably, $Li_3V_2(PO_4)_3 \leftrightarrow Li_{2.5}V_2(PO_4)_3$, $Li_{2.5}V_2(PO_4)_3 \leftrightarrow Li_2V_2(PO_4)_3$ and $Li_2V_2(PO_4)_3 \leftrightarrow LiV_2(PO_4)_3$. The four charge voltage plateaus are at 3.51 V, 3.60 V, 3.69 V and 4.08 V in Fig. 4(b), respectively. The characteristic peaks of LFP and LVP, observed in the CV curves, demonstrates that the as-prepared materials are a mixture of LFP and LVP, which is consistent with the analysis of the electron microscopy images.

Fig. 4(c) exhibits the initial charge/discharge curves of LFP–LVP/C and LFP/C between 2.5 and 4.2 V at 0.1 C. The initial discharge capacity of LFP–LVP/C is 165.2 mAh g^{-1}, which is much higher than that of many other LFP-based cathode materials reported earlier [28,11]. Yang et al. [28] prepared V-$LFePO_4$ (5% V) and show initial discharge capacities of 152.7 mAh g^{-1} at 0.1 C, and Zhang et al. [11] prepared $9LiFePO_4/C@Li_3V_2(PO_4)_3/C$ exhibiting initial discharge capacity of 162.19 mAh g^{-1} at 0.1 C. Additionally, the initial discharge capacity of as-prepared LFP/C is 144.4 mAh g^{-1}, higher than that of LFP/C (120.9 mAh g^{-1} at 0.1 C) reported by Su et al. [29]. These results show that as-prepared LFP/C and LFP–LVP/C possess excellent electrochemical performance. Furthermore, the voltage difference between the charge and discharge plateaus (ΔV) of the LFP–LVP/C (63.10 mV) is smaller than that of LFP/C (77.86 mV), indicating the polarization of LFP–LVP/C electrode is lower than that of LFP/C [30]. The lower polarization for LFP–LVP/C is ascribed to the three-dimensional NASICON-type framework structure of LVP [31], combining with V-doped LFP to improve the electrochemical performance of the LFP–LVP/C composite.

Fig. 4(d) shows discharge capacity of LFP–LVP/C and LFP/C electrodes at 1 C in the voltage range of 2.5–4.2 V. There are some pronounced scattering of the discharge capacity data, which is usually ascribed to the effect of cycling at room temperature. LFP–LVP/C exhibits excellent electrochemical performance with a specific discharge capacity of 141.6 mAh g^{-1} at 1 C after 100 cycles, which is much higher than that of LFP/C of 112.4 mAh g^{-1} after 100 cycles. There is no noticeable capacity fading on cycling for the LFP–LVP/C sample. The three-dimensional framework of LVP provides efficient three-dimensional Li^+ transport pathways and facile strain relaxation during battery charge and discharge, the synergistic effect of LFP–LVP particles and conductive carbon coating improve the performance of LFP–LVP/C, consistent with the results

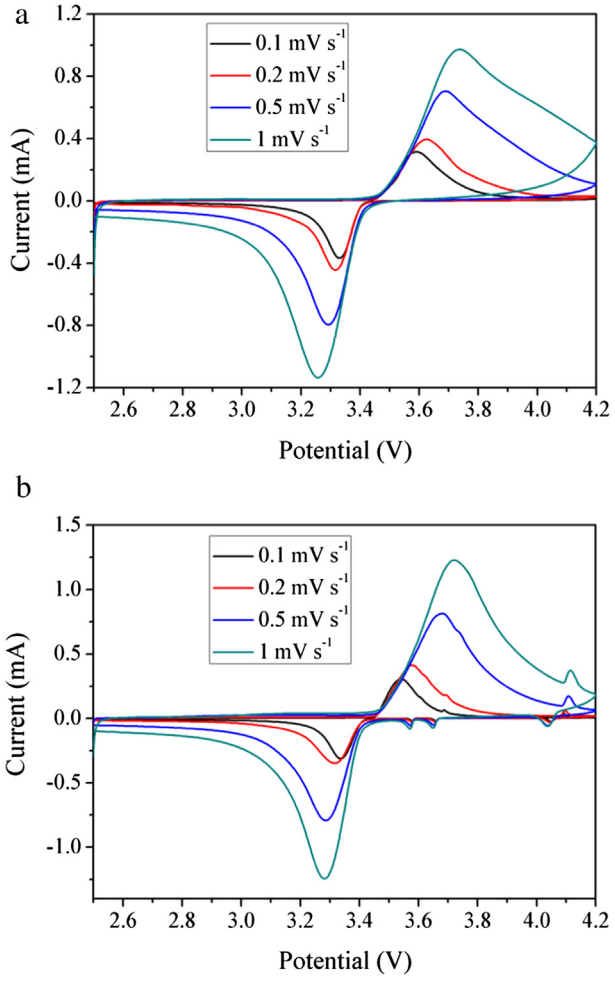

Fig. 5. Cyclic voltammograms of (a) LFP/C and (b) LFP–LVP/C in the voltage range of 2.5–4.2 V at scan rates of 0.1, 0.2, 0.5 and 1 mV s^{-1}.

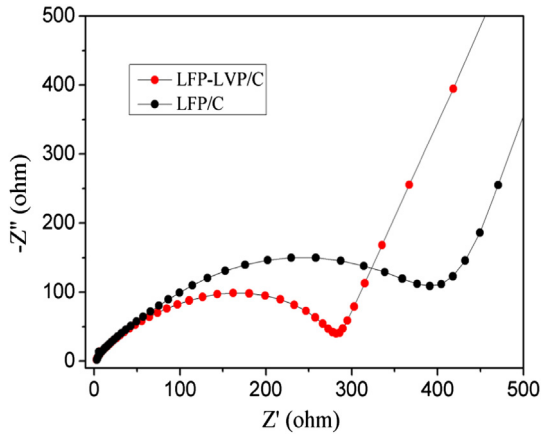

Fig. 6. Nyquist plots of LFP–LVP/C and LFP/C electrodes in the frequency range of 0.01–100 kHz.

of the analysis of the Raman spectra and electron microscopy images.

To ulteriorly compare the electrochemical performance of LFP/C and LFP–LVP/C, cyclic voltammetry measurements are conducted at various scanning rates from 0.1 to 1 mV s^{-1} between 2.5 and 4.2 V, which are shown in Fig. 5. As the scan rates increase, the two samples show that the oxidation peaks move to higher potential, and the reduction peaks move to lower potential. Thus the potential differences between the reduction and oxidation processes increase. Because the polarization appears on the electrodes and the diffusion of Li^+ inside the electrodes cannot follow the fast scan rates [32]. But for the sample LFP–LVP/C, it exhibits smaller value of potential difference, well- defined peaks and more highly symmetrical than LFP/C, which is ascribed to the three-dimensional NASICON-type framework structure of LVP in LFP–LVP/C, it provides efficient three-dimensional Li^+ transport pathways and facile strain relaxation during battery charge and discharge, which is consistent with the results of Fig. 4.

Fig. 6 presents the AC impedance spectra of LFP–LVP/C and LFP/C electrodes. Prior to the AC impedance tests, the electrodes are activated at 0.1 C for three cycles. Each spectrum consists of a semicircle in the high- to medium-frequency region and a straight line in the low-frequency region. The depressed semicircle in high- to medium-frequency region is attributed to the charge-transfer resistance (R_{ct}) of the electrochemical reaction and the straight line is related to the diffusion-controlled Warburg impedance [33]. The diameter of the depressed semicircle for LFP/C is larger than that for LFP–LVP/C, which indicates that the charge-transfer resistance of LFP–LVP/C is much lower than that of LFP/C. This reenforces the synergistic effect of LFP–LVP particles and carbon coating facilitating the charge transfer in the electrodes, and this combination resulting in the improvement of the electrochemical performance of LFP–LVP/C electrodes relative to LFP/C.

4. Conclusion

LFP–LVP/C composite is prepared by a modified solid-state method. The LFP–LVP/C composite is well crystallized with no evidence of impurities. LFP–LVP/C differs from LFP/C by featuring V-doping into the LFP structure (bulk doping) and mixed phase regions of V-doped LFP and LVP. The electrochemical performance indicates that the initial discharge capacity of LFP–LVP/C is 165.2 mAh g^{-1} at 0.1 C and more importantly, it exhibits a specific discharge capacity of 141.6 mAh g^{-1} with no noticeable capacity fading up to 100 cycles at a constant current density of 1 C, which is higher than that of as-prepared LFP/C by the same method. The improvement in the performance of LFP–LVP/C electrodes relative to LFP/C is due to the synergistic effect of V-doped LFP and LVP formation in combination with the nanoscale carbon matrix. The carbon matrix also enhances the performance of LFP/C electrodes.

Acknowledgments

This work was supported by the Program for New Century Excellent Talents in University (NCET-12-1076), the National Natural Science Foundation of China (21161021), the Australian Research Council (ARC) through a Discovery project (DP1094261) and the Program for Changjiang Scholars and Innovative Research Team in University of Ministry of Education of China (no. IRT1081). Dr. Sharma would like to thank AINSE Ltd for providing financial assistance through the Research Fellowship Scheme. The authors also would like to thank Dr. Tania Silver at the University of Wollongong for critical reading of the manuscript.

References

[1] A.K. Padhi, K.S. Nanjundaswamy, J.B. Goodenough, J. Electrochem. Soc. 144 (1997) 1188.
[2] A.R. Cho, J.N. Son, V. Aravindan, H. Kim, K.S. Kang, W.S. Yoon, W.S. Kime, Y.S. Lee, J. Mater. Chem. 22 (2012) 6556.
[3] Z.L. Gong, Y. Yang, Energy Environ. Sci. 4 (2011) 3223.
[4] X.C. Wang, Y.D. Huang, D.Z. Jia, Z.P. Guo, D. Ni, M. Miao, J. Solid State Electrochem. 16 (2010) 17.
[5] Y.H. Huang, J.B. Goodenough, Chem. Mater. 20 (2008) 7237.
[6] M.M. Ren, Z. Zhou, Y.Z. Li, X.P. Gao, J. Yan, J. Power Sources 162 (2006) 1357.
[7] M. Sato, H. Ohkawa, K. Yoshida, M. Saito, K. Uematsu, K. Toda, Solid State Ionics 135 (2000) 137.
[8] S.-C. Yin, P.S. Strobel, H. Grondey, L.F. Nazar, Chem. Mater. 16 (2004) 1456.
[9] J. Ma, B.H. Li, H.D. Du, C.J. Xu, F.Y. Kang, J. Solid State Electrochem. 158 (2011) A26.
[10] M.R. Yang, W.H. Ke, S.H. Wu, J. Power Sources 165 (2007) 646.
[11] X.P. Zhang, H.J. Guo, X.H. Li, Z.X. Wang, L. Wu, Solid State Ionics 212 (2012) 106.
[12] Y.D. Huang, R.R. Jiang, D.Z. Jia, Z.P. Guo, Mater. Lett. 65 (2011) 3486.
[13] Z.F. Dong, Y.D. Huang, R.R. Jiang, D.Z. Jia, Z.P. Guo, J. Solid State Electrochem. 15 (2011) 725.
[14] L. Wang, Y.D. Huang, R.R. Jiang, D.Z. Jia, Electrochim. Acta 52 (2007) 6778.
[15] Y.D. Huang, L. Wang, D.Z. Jia, S.J. Bao, Z.P. Guo, J. Nanopart. Res. 15 (2013) 1549.
[16] A.C. Larson, R.B. Von Dreele, Los Alamos National Laboratory Report LAUR 86-748, 1994.
[17] B.H. Toby, J. Appl. Crystallogr. 34 (2001) 210.
[18] C.-Y. Chiang, H.-C. Su, P.-J. Wu, H. Liu, C.-W. Hu, N. Sharma, V.K. Peterson, H.-W. Hsieh, Y.-F. Lin, W.-C. Chou, C.-H. Lee, J.-F. Lee, B.-Y. Shew, J. Phys. Chem. C 116 (2012) 24424.
[19] X.H. Rui, N. Ding, J. Liu, C. Li, C.H. Chen, Electrochim. Acta 55 (2010) 2384.
[20] N. Zouari, M.B. Amor, T. Mhiri, A. Daoud, J.M. Béau, J. Alloys Compd. 240 (1996) 70.
[21] L.L. Ge, C.X. Han, L.P. Ni, J. Zhang, Y.L. Tao, Q.B. Yu, Y.H. Shen, A.J. Xie, L. Zhu, Y.P. Zhang, Solid State Ionics 14 (2012) 864.
[22] Y.L. Liu, C.X. Pan, J.B. Wang, J. Mater. Sci. 39 (2004) 1091.
[23] T. Muraliganth, A. Vadivel Murugan, A. Manthiram, Chem. Commun. 47 (2009) 7360.
[24] N. Sharma, G. Du, Z. Guo, J. Wang, Z. Wang, V.K. Peterson, J. Am. Chem. Soc. 134 (2012) 7867.
[25] N. Böckenfeld, R.-S. Kühnel, S. Passerini, M. Winter, A. Balducci, J. Power Sources 196 (2011) 4136.
[26] X.B. Hu, Z.J. Lin, L. Liu, Y.J. Huai, Z.H. Deng, J. Serb. Chem. Soc. 75 (2010) 1259.
[27] H. Tang, X.D. Guo, B.H. Zhong, H. Liu, Y. Tang, R. Xu, L.Y. Li, J. Solid State Electrochem. 16 (2012) 1537.
[28] G. Yang, C.Y. Jiang, X.M. He, J.R. Ying, F.P. Cai, Ionics 18 (2012) 59.
[29] C. Su, X.D. Bu, L.H. Xu, J.L. Liu, C. Zhang, Electrochim. Acta 64 (2012) 190.
[30] Y. Zhang, W.C. Wang, P.H. Li, Y.B. Fu, X.H. Ma, J. Power Sources 210 (2012) 47.
[31] L.N. Wang, Z.C. Li, H.J. Xu, K.L. Zhang, J. Phys. Chem. C 112 (2008) 308.
[32] H.D. Liu, G. Yang, X.F. Zhang, P. Gao, L. Wang, J.H. Fang, J. Pintoc, X.F. Jiang, J. Mater. Chem. 22 (2012) 11039.
[33] F. Nobili, F. Croce, B. Scrosati, R. Marassi, Chem. Mater. 13 (2001) 1642.